

# Feasibility of Passive Wireless Sensors Based on Reflected Electro-Material Signatures

Azhar Hasan, Andrew F. Peterson, and Gregory D. Durgin

School of Electrical and Computer Engineering  
Georgia Institute of Technology, Atlanta, GA 30332-0250, USA  
azhar.hasan@gatech.edu, peterson@ece.gatech.edu, durgin@ece.gatech.edu

**Abstract**— In this paper, a neural network is applied to reconstruct the permittivity profile of a three-section passive sensor for RFID applications. Input reflection coefficients of the wave backscattered from a RF tag, over the frequency range 1-5 GHz, are used to estimate the material parameters. A neural network incorporating the Levenberg Marquardt algorithm is evaluated in terms of average absolute error, regression analysis and computational efficiency. Suitability of the algorithm is verified using both simulated and measured data, and accurate results are obtained while avoiding computational complexity. The methodology developed in this paper can be successfully used for passive sensing applications involving RFID technology to investigate and reconstruct a material profile altered by environmental variables.

**Index Terms**— RFID, sensors, neural networks, inverse scattering

## I. INTRODUCTION

Radio frequency identification (RFID) has been successfully used across a number of tracking and sensing applications. Recent development of materials whose permittivity parameters can change significantly with environmental conditions suggests the possibility of constructing a passive RFID sensor that can be interrogated remotely to extract data about the environment at the sensor [1]. A simple passive sensor of this type consists of an antenna attached to a microstrip transmission line, which in turn is routed over one or more sections of variable permittivity material before being terminated in a load. In the following, we explore the feasibility of reconstructing the permittivity profile of a three-section sensor of this type by using the backscatter from this sensor over frequencies in the range 1 - 5 GHz. Neural networks are employed to re-create the permittivity profile from the received data.

The problem of identifying medium properties from waves reflected from a device of this type is a form of the classical one dimensional inverse scattering problem. For profile inversion in a lossy inhomogeneous media, analytical techniques are difficult to implement in most practical situations,

and thus various numerical techniques have been investigated [2]. Researchers have been employing methods such as the finite difference time domain technique [3] and 1-port and 2-port measurements [4] for extracting the material properties from the information contained in reflected or transmitted waves. Artificial neural networks have been employed across a wide field of applications, including inverse electromagnetic problems [5], [6], and [7]. Exploiting a priori knowledge of the geometry, neural networks incorporating a backpropagation algorithm were able to retrieve the radius position and dielectric permittivity of a circular cylinder [8]. Neural networks have also demonstrated the ability to reconstruct the permittivity profile of homogeneous cylinders in free space and detecting the position of cylinders [9]. The effective use of neural networks to determine non-smooth, one-dimensional profiles of an inhomogeneous layer has been investigated with noisy data by Yaman and Simcsek [10].

The sensor is explained in the following section. The complex reflection coefficient is calculated using signal flow theory as described in section III. A brief introduction to neural networks, with details on the specific approach used in this investigation, is given in section IV. The feasibility study and results are demonstrated in sections V and VI.

## II. REMS SENSOR CONCEPT

A sensor concept based on reflected electro-material signatures (REMS) consists of three distinct components working together to provide passive sensing capability of environment information. The first component is the electro-material line, a chemical strip sandwiched between the ground plane and top trace of an RF tag's microstrip transmission line. The second component, the reflector circuitry, consists of the transmission line itself, the radio-frequency integrated circuit (RFIC) that performs backscatter and identification functions, and any RF tag antennas. Finally, an RF reader must be used to interrogate the REMS sensor as well as performs the signal-processing for data extraction. These components are illustrated in Fig. 1

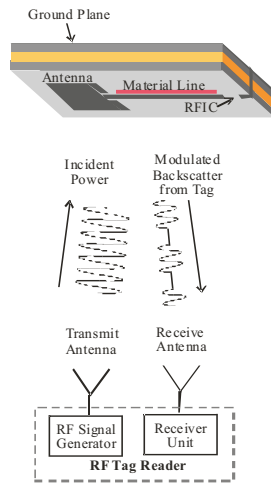


Fig. 1. Components of a REMS Sensor.

Conceivably, the REMS concept could be implemented with existing UHF or microwave passive RFID integrated circuits, greatly lowering cost and allowing passive interrogation of the sensor. In a conventional backscatter RFID system, the signal is reflected from a binary-switched load, providing two potential frequency-dependent measurements for extracting material line parameters [11]. Since an RFID reader filters out unmodulated scatter components, an RFID-based REMS sensor would allow a much more precise measurement compared to other forms of remote sensing.

Any material that has environmental sensitivity to permeability, permittivity, or conductivity may be a candidate for the electro-material line in the REMS sensor. For example, a simple instantaneous temperature sensor could incorporate thermotropic liquid crystals. These types of liquid crystals experience state disordering upon heating, leading to a change in their electrical (and optical) properties [12, 13]. A common, everyday example of these liquid crystals are the disposable thermometer magnets that allow temperature readouts to become visible through a graded liquid crystal film. Another example of candidate material may be a line substrate doped with ferroelectric or super-paramagnetic particles [14]. Such a device could use the nonlinear relationship between field and flux density components to sense external field strengths. The REMS sensor concept may also allow for materials that time-record environmental attributes, thus providing a form of chemical memory rather than electrical memory that would achieve a completely passive sensor. This type of sensor functionality cannot be achieved under today's 'system on a chip' paradigm, which still requires external power supplies for electronic memory recording functions.

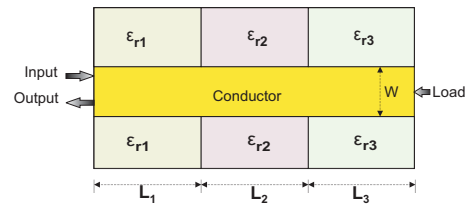


Fig. 2. The microstrip line model with three discrete segments having different permittivity profiles, terminated in a load to emulate a REMS sensor with three wells of sensor material.

### III. CALCULATING REFLECTION COEFFICIENT FROM TRANSMISSION LINE MODEL

A REMS reader is an RF transceiver that measures modulated backscatter signals from the RF tag. To test the REMS concept, the sensor is modeled using three cascaded microstrip transmission lines, emulating a three part step discontinuity in the electro-material line. Each cascaded microstrip line is 1.25cm long and 0.5cm wide with a substrate height of 0.05cm. Different dielectric materials in the segments are used to emulate a REMS sensor with three wells of sensor material. The line is terminated in a resistive load. As the transmission line geometry is not specifically designed for a characteristic impedance of  $50\Omega$ , this load causes part of the wave to be absorbed and part reflected back. The microstrip line model with three discrete segments having different permittivity profiles is shown in Fig. 2. For the frequency range of 1-5GHz, the relative permittivity,  $\epsilon_r$ , of each segment was swept across a range of values, and the values of reflection coefficient,  $\Gamma_{IN}$ , at the input of the system were computed. Each transmission line acts as a two port network, and the complete system of the cascaded lines can be analyzed in terms of S-parameters and signal flow graphs [15], using Eq. 1.

$$\Gamma_{IN} = \frac{b_1}{a_1} = S_{11} + \frac{S_{12}S_{21}\Gamma_L}{1 - S_{22}\Gamma_L} \quad (1)$$

The complex-valued reflection coefficient contains information about magnitude as well as phase, and both will be used by the inversion algorithm. To demonstrate how the frequency-swept measurement of an RF reader changes for slight perturbations in the permittivity profiles, the dielectric constant of the second bin was changed for four different values, as illustrated in Fig. 3, and the reflection coefficient was calculated for each case. The effect on magnitude and phase of  $\Gamma_{in}$ , between four values of  $\epsilon_{r2}$ , with  $\epsilon_{r1} = 2.5$  and  $\epsilon_{r3} = 3.5$ , is shown in Fig. 4 and Fig. 5, respectively. Significant alterations are observed in the magnitude and phase

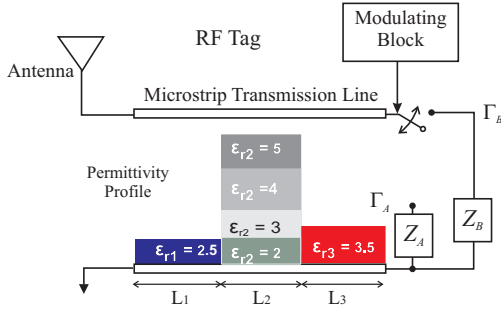


Fig. 3. The transmission line model of the RF tag, illustrating four changing permittivity profiles of the center well of the REMS sensor.

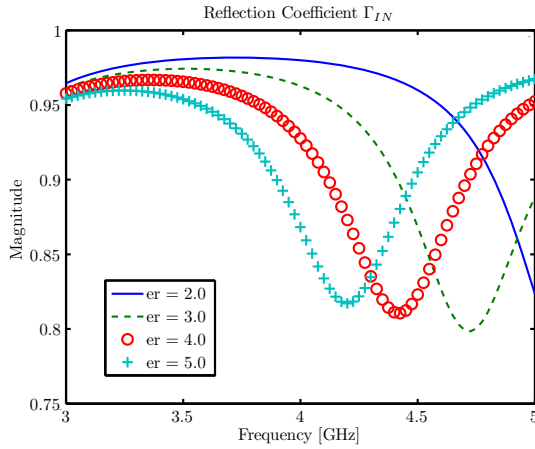


Fig. 4. Magnitude of  $\Gamma_{IN}$  for  $\epsilon_{r2} = 2, 3, 4$  and  $5$  calculated from the signal flow graph.

of the wave scattered out of the tag. Theoretically, every material profile will produce a unique frequency sweep - although designing a wide range of switchable loads ( $Z_A$ ,  $Z_B$ , and possible more) will greatly affect measurement resolution and sensitivity.

#### IV. NEURAL NETWORK

The idea of neural networks evolved in late 19th century in an attempt to understand how the human brain functions. The concept of decentralized network units (neurons) was introduced in 1943 when McCulloch and Pitts developed the first mathematical model of a neuron [16]. Inspired from brain function, the neural network is generally used to solve artificial intelligence problems without requiring a model of the system. Neural networks are adjusted and trained to solve problems that are difficult to solve using conventional techniques and are extremely useful in pattern recognition and function approximation problems. In this paper, a neural

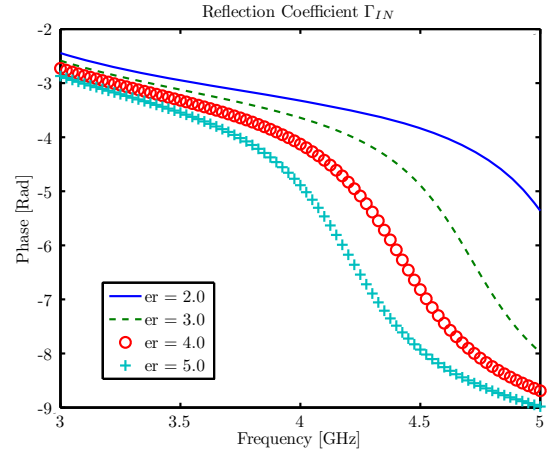


Fig. 5. Phase of  $\Gamma_{IN}$  for  $\epsilon_{r2} = 2, 3, 4$  and  $5$  calculated from the signal flow graph.

network is used to extract the material properties of the microstrip transmission line structure based on the reflection coefficient of a backscattered wave.

In a typical single neuron having a scalar input  $p$ ,  $p$  is multiplied with a weight  $w$  and added to a bias/offset  $b$ . A neuron may or may not have the bias/offset. The output  $n$  (net input) of the summer forms the argument of an activation function (transfer function)  $f$ , whose output  $a$  is the output of the neuron. The activation function is chosen by the designer, while the weight and bias (if used) are adjusted by some learning rule [17]. The output function is described by Eq. 2.

$$a = f(wp + b) \quad (2)$$

For many systems, one neuron is insufficient and therefore multiple neurons and multiple neuron layers are used, as depicted in Fig. 6. For one such layer comprising  $S$  neurons, there may be an arbitrary number of inputs  $R$ , each connected to all  $S$  neurons. The resulting weight matrix has dimension  $S \times R$ . The number of neurons is independent of the number of rows and columns [17]. All neurons usually have the same transfer function, although this is not always the case [17]. In the event that one layer of multiple neurons is inadequate, a network with additional (hidden) layers can be used. Each layer has its own weight matrix  $W$ , bias vector  $b$ , net input vector  $n$  and output vector  $a$ . For  $R$  inputs and  $S^1$  neurons in the first layer, the second layer can be considered as a layer with  $S^1$  inputs,  $S^2$  neurons and a weight matrix of order  $S^1 \times S^2$ . Input to the second layer is  $a^1$  and its output is the input to the next layer. The final output,  $a^3$ , is given by

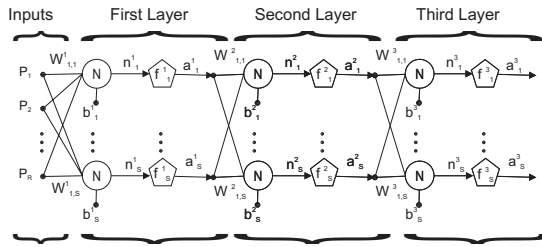


Fig. 6. Three layers of multiple neurons.

Eq. 3.

$$a^3 = f^3(W^3 f^2(W^2 f^1(W^1 p + b^1) + b^2) + b^3) \quad (3)$$

The transfer function may be linear or nonlinear depending upon the problem. The three most commonly used transfer functions are the *hardlimit* transfer function, the *linear* transfer function, and *logsigmoidal* transfer function [16]. The logsigmoidal transfer function takes an input from minus infinity to plus infinity and compresses the output into the range 0 to 1 according to the expression in Eq. 4. It is the most typically used transfer function in backpropagation algorithms and is used in this work as well.

$$a = \frac{1}{1 + e^{-n}} \quad (4)$$

### A. Training Algorithms

The weights described in the previous section must be determined by a training process that attempts to match the actual output of the neural network with the desired output for a training data set. Function approximation problems are typically solved using backpropagation algorithms, which require the activation function to be differentiable. A common implementation is known as the *delta* rule, given by Eq. 5 for the  $j^{\text{th}}$  neuron and the  $i^{\text{th}}$  weight, where  $\alpha$  is the constant learning rate,  $t_j$  is the target output,  $y_j$  is the actual output and  $g(x)$  is the activation function.

$$\Delta w_{ji} = \alpha(t_j - y_j)g'(h_j)x_i \quad (5)$$

Eq. 5 provides the adjustment in weights during one step of the training process.

The training algorithm must minimize the error between the desired and actual network outputs as quickly as possible. The learning rate (denoted by  $\alpha$  or  $l_r$ ) is a critical parameter in every algorithm. If  $l_r$  is too large, the algorithm may be unstable, and if  $l_r$  is too small, the algorithm converges too slowly. A variety of heuristic or numerical optimization algorithms are reported in the literature [17, 18, 19, 20, 21, 22]. Each algorithm has its own merits

and demerits depending upon the type of problem and computing resources. The gradient descent and gradient descent with momentum algorithms are considered too slow for practical problems [17]. Conjugate gradient methods were invented purely for quadratic functions, and some require excessive memory while others require more iterations to converge. Newton's method is an alternative to conjugate gradient methods for fast optimization, and often converges faster than the conjugate gradient method, but it involves the Hessian which is expensive to compute. In the quasi-Newton method, an approximate Hessian is updated at each iteration instead of being recomputed from scratch [17]. The Broyden, Fletcher, Goldfarb, and Shanno (BFGS) algorithm requires more computation and storage than the conjugate gradient algorithm and is not suited to large networks [17]. The one step secant algorithm is an effort to bridge the gap between conjugate gradient and quasi-Newton algorithms. In terms of accuracy (mean square error), speed, and memory requirements, which algorithm performs best depends upon a number of factors including the problem complexity, the number of points in the data set, weights, biases, the desired accuracy, and the type of problem (pattern recognition or function approximation). For a function approximation problem having a network with a few hundred weights, the Levenberg Marquardt (LM) algorithm often converges the fastest [17].

A number of simulations were carried out to determine the best algorithm, with the result that the LM algorithm exhibited superior absolute average error and computation time. The algorithm was designed to approach second order training speed without computing the Hessian  $H$ , instead using the approximation  $H = J^T J$ , where  $J$  is the Jacobian containing the first derivative of network errors with respect to weights and biases. The gradient is computed as  $g = J^T e$ , where  $e$  is the vector of network errors [23]. The Jacobian is computed through a standard back propagation technique which is much less complex than computing the Hessian [24]. The algorithm may be written as

$$x_{k+1} = x_k - [J^T J + \mu I]^{-1} J^T e \quad (6)$$

The primary drawback of the Levenberg Marquardt algorithm is that it requires the storage of a relatively large matrix. The size of the Jacobian is  $Q \times n$ , where  $Q$  is the number of training sets and  $n$  is the number of weights and biases. The Jacobian can be divided into equal sub matrices, with the Hessian expressed as

$$H = J^T J = J_1^T J_1 + J_2^T J_2 \quad (7)$$

Table 1. Comparison of actual values of  $\epsilon_{r1,2,3}$  vs neural network output

	Actual Values	Neural Network output	Error
Set1	4	4.115	0.115
	4	4.024	0.024
	4	3.985	-0.015
Set2	2	2.018	0.018
	2.3	2.334	0.034
	4.8	4.501	-0.299
Set3	3	3.255	0.255
	2.5	2.495	0.005
	4.5	4.238	0.262

Table 2. Dimensions of microstrip transmission lines in experimental setup.

	Trnas Line 1	Trans Line 2	Trans Line 3
Length (L)	1.25 cm	1.25 cm	1.25 cm
Width (W)	0.5 cm	0.5 cm	0.5 cm
Substrate Height	0.127 cm	0.157 cm	0.127 cm
Conductor Thickness	0.0017 cm	0.0017 cm	0.0017 cm
Loss Tangent	0.002	0.0009	0.002
Substrate	RO 3006	RT/Duroid 5880	RO 3006
Dielectric Constant	6.15	2.2	6.15

Table 3. Comparison of values of  $\epsilon_{r1,2,3}$  estimated using neural networks against the actual values for frequency range 1-2.5 GHz.

	$\epsilon_{r1}$	$\epsilon_{r2}$	$\epsilon_{r3}$	Average Error
Actual Value	6.15	2.2	6.15	
Estimate 1 using LM Algorithm	5.72	2.73	5.60	
Absolute Error	0.43	0.53	0.55	0.50
Estimate 2 using LM Algorithm	5.72	2.89	5.53	
Absolute Error	0.43	0.69	0.62	0.58
Estimate 3 using LM Algorithm	5.67	2.81	5.69	
Absolute Error	0.48	0.61	0.46	0.51

where  $J$  is divided into two equal matrices  $J_1$  and  $J_2$ .

## V. APPLICATION OF NEURAL NETWORKS FOR EXTRACTING MATERIAL PROPERTIES ( $\epsilon_R$ )

As a first step in using a neural network to extract material parameters, the dielectric constant  $\epsilon_{r2}$  of the center segment of a 3-step microstrip line is varied from 2-8 with a step size of 0.1, while  $\epsilon_{r1}$  and  $\epsilon_{r3}$  were fixed at 3 and 3.8, respectively. A data set containing the magnitude and phase of  $\Gamma_{in}$  was generated for frequencies from 5 to 6 GHz with a step size of 100 MHz. The step size of 100 MHz was chosen to keep the data matrix dimensions within the computing capability of a modest desktop computer; it was observed that frequency steps smaller than 100MHz did not increase the accuracy of the results. The magnitude and phase values were combined in the data matrix  $D$ , which has the form shown in Eq. 8.

$$D = \begin{bmatrix} |\Gamma| \\ \angle\Gamma \end{bmatrix} \quad (8)$$

For the initial test,  $|\Gamma|$  and  $\angle\Gamma$  were matrices of dimensions  $11 \times 61$ , corresponding to 11 frequencies and 61 different values of  $\epsilon_{r2}$ . A finer increment of the dielectric constant, 0.01 for instance, might improve the accuracy of the network model, but at a cost of increasing each matrix to  $11 \times 601$ . The neural network with 10 neurons in single layer was trained using  $\epsilon_{r2}$  in the range from 2-8, and then tested using the phase and magnitude of  $\Gamma_{in}$  corresponding to  $\epsilon_{r2} = 2.1$ , and 4.75. The network produced estimated values for  $\epsilon_{r2}$  of 2.1186 and 4.7693, respectively.

As a second test,  $\epsilon_{r1}$  and  $\epsilon_{r3}$  were also varied as the frequency was swept across the 5-6 GHz range with a step size of 100 MHz. Values of  $\epsilon_{r1}$ ,  $\epsilon_{r2}$ , and  $\epsilon_{r3}$  were varied from 2-5 with a step size of 0.1. The resulting data matrix had dimensions  $22 \times 29,971$ . After training, the Levenberg Marquardt algorithm

with 10 neurons in a single layer was able to produce relative permittivity values within  $\pm 0.3$  of the actual values, as summarized for several examples in Table 1.

The first two tests were carried out with a single neuron layer. Additional tests were carried out with single layer networks with 5, 10, 15, 20 and 25 neurons, and a two layer network with 10 neurons each. The results were compared in terms of error and coefficient of regression analysis. Each network was tested for the set of permittivity values shown in Eq. 9 in matrix  $T$ . The rows of  $T$  correspond to  $\epsilon_{r1}$ ,  $\epsilon_{r2}$  and  $\epsilon_{r3}$ , while the columns show the set of dielectric constants presented to the network at each time. It was observed that a single layer with 20 or 25 neurons is best suited in terms of absolute mean error and computation efficiency. The errors for 20 neurons are shown in matrix  $E_{20}$  in Eq. 10.

$$T = \begin{bmatrix} 2.1 & 2.5 & 3.5 \\ 3.5 & 3.5 & 3 \\ 4.9 & 4.5 & 4 \end{bmatrix} \quad (9)$$

$$E_{20} = \begin{bmatrix} -0.097 & -0.026 & 0.005 \\ 0.048 & 0.004 & 0.015 \\ -0.015 & 0.008 & 0.009 \end{bmatrix} \quad (10)$$

To simulate the presence of white Gaussian measurement noise, random numbers were added to the training data. Five different levels of noise corresponding to a 5dB, 10dB, 15dB, 20dB and 30dB signal to noise ratio (SNR) were induced. The system was trained, validated and tested using the LM algorithm, and regression analysis was carried out. The coefficient of correlation from regression analysis for all different levels of SNR is plotted in Fig. 7 where it can be observed that higher SNR corresponds to higher coefficient of regression  $R$  and vice versa. The ideal value for  $R$  is 1.0.

## VI. EXPERIMENTAL MEASUREMENT AND ANALYSIS

To enable measurements, a device was fabricated with three microstrip transmission lines cascaded together in the fashion described in section III, as shown in Fig. 2 and Fig. 8. The dimensions and dielectric properties of the cascaded microstrip lines are tabulated in Table 2. Materials with parameter values of  $\epsilon_{r1} = \epsilon_{r3} = 6.15$  and  $\epsilon_{r2} = 2.2$  were used. The microstrip line was terminated in a  $50\Omega$  load.

A network analyzer was used to record S-parameters over the frequency range 1-5 GHz. A comparison between measured and simulated values of the magnitude and phase of the reflection coefficient are shown in Figs. 9 and 10. There is

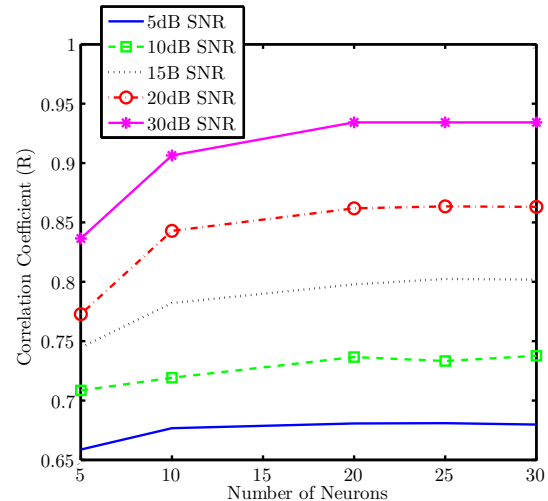


Fig. 7. Correlation coefficient ( $R$ ) of regression analysis plotted against the number of neurons for a network trained with data having white Gaussian noise. Number '30' on the X-axis represents two hidden layers of 10 neurons each



Fig. 8. Snapshot of microstrip transmission line setup for experimental measurements.

excellent agreement between measured and simulated results in the frequency range 1-2.5 GHz, and reasonable agreement at higher frequencies. Ripples and other deviations are observed for higher frequencies, which can be attributed at least in part to discontinuities introduced by the fabrication technique. The microstrip lines were soldered together horizontally, across the width, which caused a noticeable amount of solder paste to sit on the joints. Moreover, a thin wire was also inserted horizontally to strengthen the solder.

For training purposes, simulated data was generated for  $\epsilon_{r1}$  and  $\epsilon_{r3}$  swept across the range from 5 - 8, and for  $\epsilon_{r2}$  from 1.1 - 3.6. This results in a dataset with  $30 \times 25 \times 30 = 22,500$  vectors. The row dimension of the data matrix is determined by frequency range and frequency step size. To limit

Table 4. Comparison of actual values of  $\epsilon_{r1,2,3}$  with the neural network results obtained with 1 layer of 20 neurons and trained on data having different levels of white noise, over the frequency range from 1-5 GHz.

	'R'	$\epsilon_{r1}$	$\epsilon_{r2}$	$\epsilon_{r3}$	Average Error
Actual Value		6.15	2.2	6.15	
Estimated with AWGN (30dB SNR)	0.99	5.96	2.56	7.23	
Absolute Error		0.19	0.36	1.08	0.54
Estimated with AWGN (20dB SNR)	0.952	5.91	2.96	6.58	
Absolute Error		0.24	0.76	0.43	0.48
Estimated with AWGN (10dB SNR)	0.956	5.95	2.75	6.20	
Absolute Error		0.20	0.55	0.05	0.27
Estimated with AWGN (05dB SNR)	0.91	6.45	2.75	6.04	
AbsoluteError		0.30	0.55	0.11	0.32

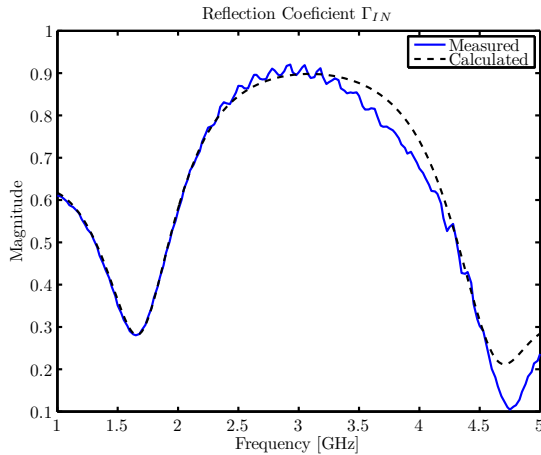


Fig. 9. Comparison between magnitude of measured and calculated reflection coefficient ( $|\Gamma_{in}|$ ).

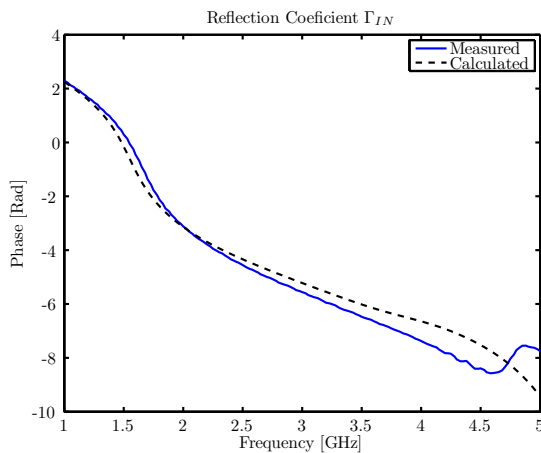


Fig. 10. Comparison between measured and calculated phase of reflection coefficient ( $\angle\Gamma_{in}$ ).

the column length, the frequency range from 1-2.5 GHz was used. A neural network containing a single hidden layer of 20 neurons was trained with data containing white Gaussian noise (10dB SNR). To eliminate the element of coincidence, and verify the robustness of algorithm, the neural network was trained and tested three times on the same data, with different starting weights each time. The three sets of results are tabulated in Table 3. These results exhibit an average absolute error range of  $\pm 0.6$  and a coefficient of regression R greater than 0.92.

Additional tests were carried out using the 1-5 GHz frequency range, with a frequency step size of 300 MHz. Using 20 neurons with the LM algorithm, a neural network was trained with simulated data containing white Gaussian noise. In terms of absolute error, the coefficient of regression R was determined to be 0.91, 0.95, 0.95 and 0.99 for an SNR of 5, 10, 20 and 30 dB, respectively. Table 4 shows the estimated values of dielectric constants and their absolute error levels. In this case, the best errors are achieved for a neural network trained with a data set containing white Gaussian noise with an SNR of 10dB. To verify the optimum number of neurons in the hidden layer, the same procedure was repeated for 25 neurons, with similar results for the coefficient of regression as a function of the SNR level. In this case 20 neurons is sufficient for an accurate approximation using a frequency range from 1-5GHz and a step size of 300 MHz.

### VII. CONCLUSION

In this feasibility study, neural networks were used to extract material parameter values from reflection coefficient data obtained from an RFID-like sensor. The dielectric constant was varied across each of three lengths of microstrip transmission lines. With a priori knowledge of geometry of the structure and the range of varying dielectric constants, the neural network was trained with data for the magnitude and phase of  $\Gamma_{in}$  across the complete frequency range of interest. The frequency resolution was an important parameter for accu-

racy of results and computational efficiency. It was demonstrated that a frequency step size smaller than 100 MHz does not improve the accuracy of results. Furthermore, for a wide range of frequencies from 1-5 GHz, a frequency resolution of 300MHz is sufficiently dense to keep the results accurate while maintaining the computational efficiency of the algorithm. The Levenberg Marquardt backpropagation algorithm was determined to be well-suited to solve this one dimensional inverse scattering type problem using neural networks. White Gaussian noise with a 10dB SNR was induced in training data to simulate the measurement noise. The architecture of the neural network is an important parameter for any problem, and it was demonstrated that one hidden layer of 20 or 25 neurons enables optimum performance of the network in terms of average absolute error and computational efficiency. With the application of a neural network based on the LM backpropagation algorithm with one hidden layer of 20 neurons, the dielectric constant of a three cascaded microstrip transmission line system was estimated with absolute average error less than  $\pm 0.5$ . We note that this one dimensional inverse scattering problem would be more challenging to investigate with non deterministic boundaries and for material properties that vary across a greater range.

## REFERENCES

- [1] G. Durgin, "Reflected Electro-Material Signature (REMS) Sensor," Provisional Patent filed on June 2008.
- [2] C. Q. Lee, "Wave propagation and profile inversion in lossy inhomogeneous media," *Proceedings of the IEEE*, vol. 70, no. 3, pp. 219–228, Mar. 1983.
- [3] H. W. Yang and R. S. Chen, "FDTD analysis on the effect of plasma parameters on the reflection coefficient of the electromagnetic wave," *Optical and Quantum Electronics*, vol. 39, no. 15, pp. 1245–1252, Dec. 2007.
- [4] E. Kemppinen, "Effective permittivity and attenuation coefficient of microstrip transmission line determined by 1-port and 2-port measuring methods," *Measurement Science and Technology*, vol. 11, pp. 38–44, 2000.
- [5] S. Ratnajeevan and H. Hoole, "Artificial neural networks in the solution of inverse electromagnetic field problems," *IEEE Trans. on Magnetism*, vol. 29, no. 2, pp. 1931–1934, Mar. 1993.
- [6] I. Elshafiey, L. Udpa, and S. S. Udpa, "Application of Neural Networks to Inverse Problems in Electromagnetics," *IEEE Trans. on Magnetism*, vol. 30, no. 5, pp. 3629–3632, Sep. 1994.
- [7] C. Christodoulou and M. Georgiopoulos, *Application of Neural Networks in Electromagnetics*, Boston, London: Artech House, 2001.
- [8] S. Caorsi, and P. Gamba, "Electromagnetic detection of dielectric cylinders by a neural-network approach," *IEEE Trans. on Geo Science and Remote Sensing*, vol. 37, no. 2, pp. 820–827, Mar. 1999.
- [9] E. Bermami, S. Caorsi, and M. Raffetto, "Microwave detection and dielectric characterization of cylindrical objects from amplitude-only data by means of neural networks," *IEEE Trans. on Antennas and Propagation*, vol. 50, no. 9, pp. 1309–1314, Sep. 2002.
- [10] F. Yaman and S. Simsek, "Neural network approach to determine nonsmooth one-dimensional profiles in inverse scattering theory," *Microwave and Optical Technology Letters*, vol. 49, no. 12, pp. 3158–3162, Sep. 2007.
- [11] J. D. Griffin and G. D. Durgin, "Complete Link Budgets for RFID and Backscatter Radio," *IEEE Antennas and Propagation Magazine*, vol. 51, no. 2, pp. 11–25, April 2009.
- [12] S. Chandrasekhar, *Liquid Crystals, 2nd Ed.*, Cambridge: Cambridge University Press, 1992.
- [13] P. J. Collings and M. Hird, *Introduction to Liquid Crystals*, Bristol, PA: Taylor & Francis, 1997.
- [14] R. C. O'Handley, *Magnetic Materials: Principles and Applications*, Wiley-Interscience, 1999.
- [15] D. M. Pozar, *Microwave Engineering, 3rd Ed.*, John Wiley and Sons- New York, 2005.
- [16] K. Mehrotra, S. Ranka and C. K. Mohan, *Elements of Artificial Neural Networks*, MIT Press, 1996.
- [17] M. T. Hagan, H. B. Demuth and M. Beale, *Neural Network Design*, Boston, MA: PWS Publishing Company, 1996.
- [18] D. G. Luenberger, *Introduction to Linear and Non Linear Programming*, Addison Wesley Pub. Co., 1973.
- [19] M. Powell, "Restart procedures for the conjugate gradient method," *Mathematical Programming*, vol. 12, pp. 241–254, 1977.
- [20] E. M. L. Beale, *A derivation of conjugate gradients in F. A. Lootsma, Ed., Numerical methods for nonlinear optimization*. London Academic Press, 1972.
- [21] M. Moller, "A scaled conjugate gradient algorithm for fast supervised learning," *Neural Networks*, vol. 6, pp. 525–533, 1993.
- [22] R. Battiti, "First- and Second-Order Methods for Learning: Between Steepest Descent and Newton's Method," *Neural computation*,

vol. 4, no. 2, pp. 141–166, Jun. 1992.

- [23] D. W. Marquardt, “An Algorithm for Least-Squares Estimation of Nonlinear Parameters,” *Journal of the Society for Industrial and Applied Mathematics*, vol. 11, no. 2, pp. 431–441, Jun. 1963.
- [24] M. T. Hagan and M. B. Menhaj, “Training feed-forward networks with the Marquardt algorithm,” *IEEE Transactions on Neural Networks*, vol. 5, no. 61, pp. 989–993, Nov. 1994.



**Azhar Hasan** received his BE and MS degrees in electrical engineering from National University of Sciences and Technology, Pakistan, in 1997 and 2007 respectively. He is currently working pursuing the PhD degree in electrical and computer engineering at Georgia Institute of

Technology, Atlanta.

His research involves computational techniques for passive RFID based sensing applications. He also holds interest in researching passive components for RF/microwave front end applications.



**Andrew F. Peterson** received the B.S., M.S., and Ph.D. degrees in Electrical Engineering from the University of Illinois, Urbana-Champaign in 1982, 1983, and 1986 respectively. Since 1989, he has been a member of the faculty of the School of Electrical and Computer Engineering at the Georgia Institute of Technology, where he is now Professor and Associate Chair for Faculty Development. He served for six years as a Director of ACES, and is a past President of the IEEE Antennas and Propagation Society. He is a recipient of the IEEE Third Millennium Medal, and is a Fellow of ACES and the IEEE.



**Gregory D. Durgin** joined the faculty of Georgia Tech’s School of Electrical and Computer Engineering in Fall 2003 where he serves as an associate professor. He received the BSEE (96), MSEE (98), and PhD (00) degrees from Virginia Polytechnic Institute and State University.

In 2001 he was awarded the Japanese Society for the Promotion of Science (JSPS) Post-doctoral Fellowship and spent one year as a visiting researcher with Morinaga Laboratory at Osaka University. In 1998 he received the Stephen O. Rice prize (with coauthors Theodore S. Rappaport and Hao Xu) for best original journal article in the *IEEE Transactions on Communications*. Prof. Durgin also authored *Space-Time Wireless Channels*, the first textbook in the field of space-time channel modeling. Prof. Durgin founded the Propagation Group (<http://www.propagation.gatech.edu>) at Georgia Tech, a research group that studies radiolocation, channel sounding, backscatter radio, RFID, and applied electromagnetics. He is a winner of the NSF CAREER award as well as numerous teaching awards, including the Class of 1940 Howard Ector Outstanding Classroom Teacher Award at Georgia Tech (2007). He is a frequent consultant to industry, having advised many multinational corporations on wireless technology.